Institute for Physics and Institute for Low Temperature Plasma Physics

Laboratory Course

Group		A	B	C	D	E	F	G	H
Monday	14.00-15.30	Lab1	Lab2	Lab3	Lab4	Lab5	Lab6	Lab7	Lab8
17.09.2007	15.30-16.00	Coffee							
	16.00-17.30	Lab2	Lab3	Lab4	Lab5	Lab6	Lab7	Lab9	Lab1
Tuesday	14.00-15.30	Lab3	Lab4	Lab5	Lab6	Lab7	Lab8	Lab1	Lab2
18.09.2007	15.30-16.00	Coffee							
	16.00-17.30	Lab4	Lab5	Lab6	Lab7	Lab8	Lab1	Lab2	Lab3
Wednesday	14.00-15.30	Lab5	Lab6	Lab7	Lab8	Lab1	Lab2	Lab3	Lab4
19.09.2007	15.30-16.00	Coffee							
	16.00-17.30	Lab6	Lab7	Lab8	Lab1	Lab2	Lab3	Lab4	Lab5
Thursday	14.00-15.30	Lab7	Lab8	Lab1	Lab2	Lab3	Lab4	Lab5	Lab6
20.09.2007	15.30-16.00	Coffee							
	16.00-17.30	Lab8	Lab1	Lab2	Lab3	Lab4	Lab5	Lab6	Lab7

Lab1	Probe diagnostics	Mario Hannemann	INP
Lab2	Optical Emission Spectroscopy	Kristian Dittmann	C1
Lab3	Tunable diode laser absorption spectroscopy	Hoang Tung Do	B1
Lab4	Fourier Transform Infrared Spectrometer and Infrared Spectroscopy using Quantum Cascade Lasers	Marko Hübner	INP
Lab5	Dielectric barrier discharge	Abhijit Majumdar	C0
Lab6	Magnetron plasma source	V. Stranak	C0
Lab7	X-ray Photoelectron Spectroscopy (XPS)	Stefan Wrehde	C0
Lab8	Diagnostics of plasma deposited layers by x-ray diffractometry	Marion Quaas	C3

R. Hippler

Lab1: Probe diagnostics

Mario Hannemann, INP

- Performing the measurement
  - Conditions for a simple probe measurement
  - Material and geometry of probe
  - Probe bias and current measuring range
- Particularities of probe measurements in rf-discharges
  - Rf-distortion of the characteristic and the rf-compensation
  - Probe measurement without and with rf-compensation in capacitively coupled parallel plate discharge (p: 0,3-0,5 mbar, P: 10 W)
- Simple evaluation of probe characteristics measured in DC-discharges or rf-discharges with sufficient rf-compensation, demonstration and visualization of the steps of evaluation
  - Maxwellian distribution – Non-Maxwellian distribution
  - Plasma potential $V_p = V(i'_{max}) = V(i''=0)$
  - Electron retarding current from total current using ion saturation current according to cold ion approximation
  - Electron temperature from electron retarding current with $V < V_p$
  - Electron density from probe current at plasma potential
  - Electron energy distribution function, mean energy and electron density from second derivative of probe characteristic
- Modification of evaluation at incomplete rf-compensation, demonstration and visualization
  - Plasma potential $V_p = (V(i''_{min}) + V(i''_{max}))/2$
  - Electron temperature from electron retarding current with $V < V(i''_{max})$
  - Electron density from probe current at plasma potential
  - Virtual plasma potential for evaluation of second derivative of a probe characteristic

University of Greifswald, Institute of Physics
Low-temperature Plasma Physics, Prof. Dr. J. Meichsner
Felix-Hausdorff-Str. 6, D-17487 Greifswald, Germany
http://www1.physik.uni-greifswald.de

Optical Emission Spectroscopy (OES)

Experimental Setup

Discharge – asymmetric, capacitively coupled rf-plasma (CCP) in oxygen

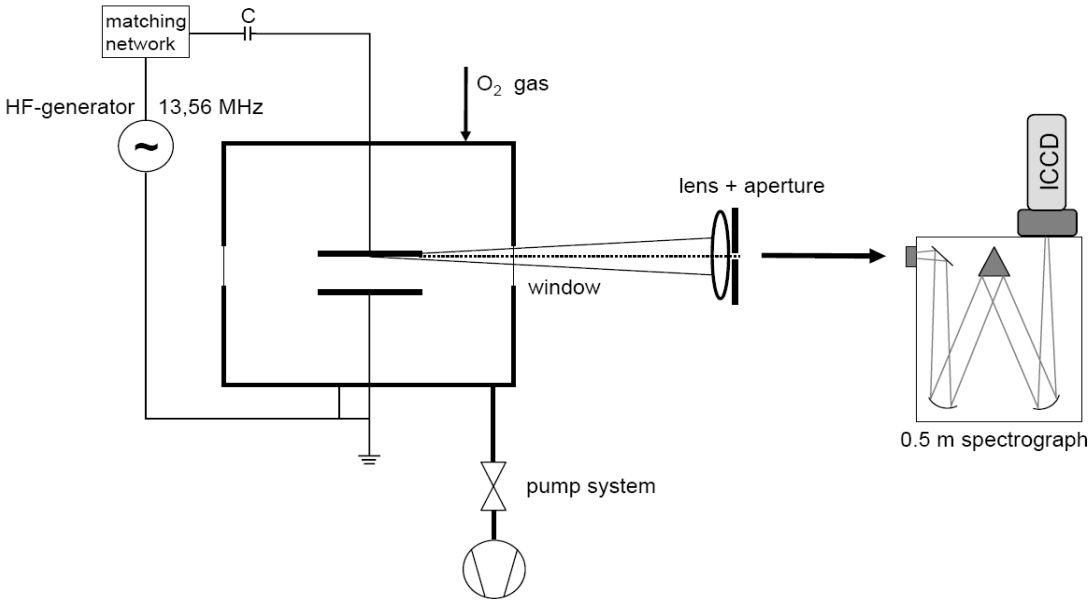

- Electrode gap d = 25 mm
- Selfbias voltage U_{Bias} = -100…-500 V
- Pressure p = 5 - 100 Pa
- Gas flow Φ = 3 sccm
- Volume V = 35 l

$n_e \sim 10^9$ cm^{-3}

$n_O \sim 10^{13}$ cm^{-3}

ICCD-Kamera (PI-MAX, Gen II RB)

axial resolution < 1 mm
spectral resolution < 0,1 nm
time resolution < 2 ns

University of Greifswald, Institute of Physics
Low-temperature Plasma Physics, Prof. Dr. J. Meichsner
Felix-Hausdorff-Str. 6, D-17487 Greifswald, Germany
http://www1.physik.uni-greifswald.de

Emission spectrum of oxygen rf plasma – 300 nm…900 nm

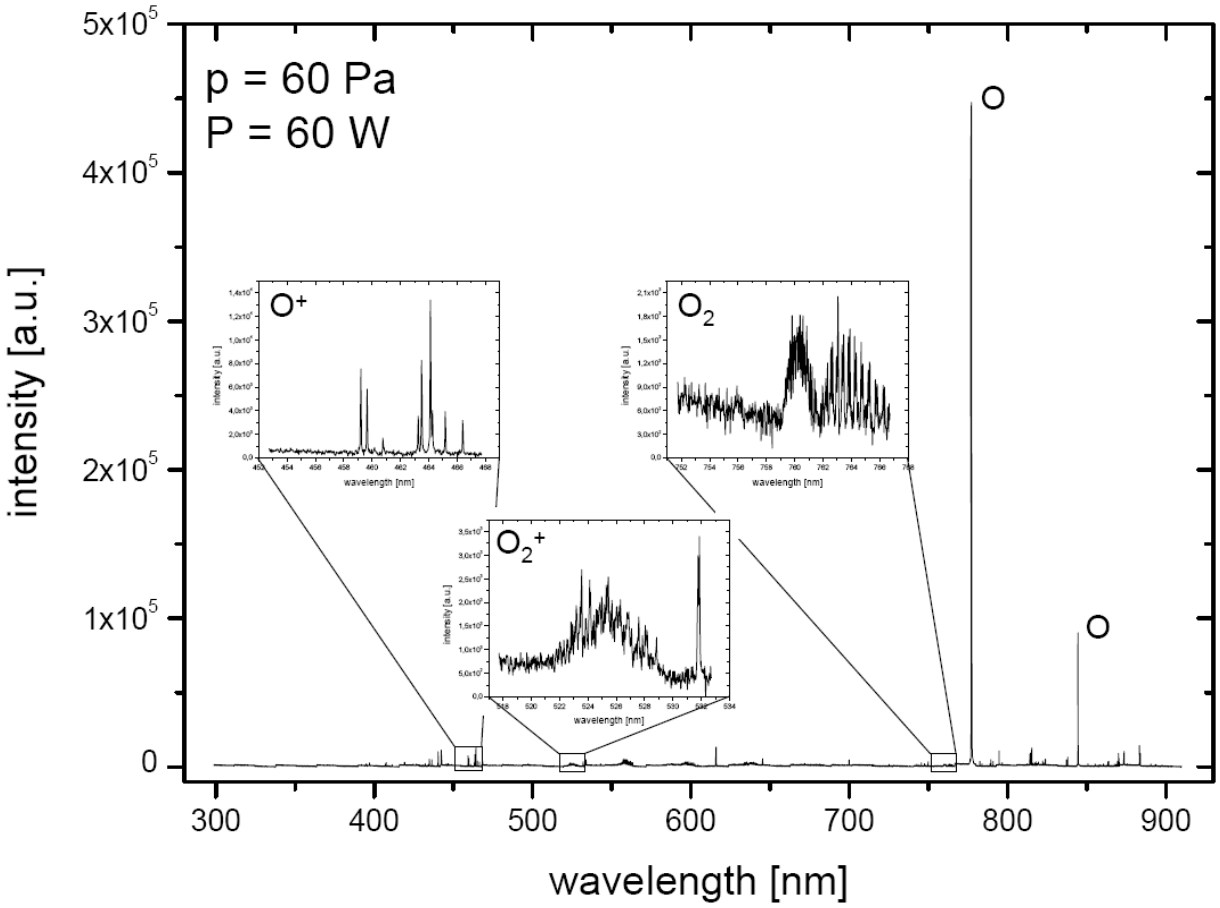

- strong emission of atomic oxygen at 777.4 nm and 844.6 nm

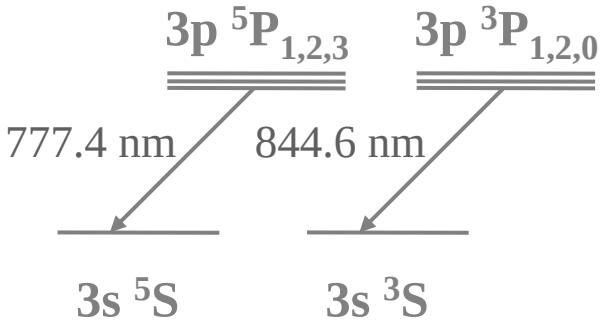

- emission of other oxygen species: O^+, O_2^+ and O_2

University of Greifswald, Institute of Physics
Low-temperature Plasma Physics, Prof. Dr. J. Meichsner
Felix-Hausdorff-Str. 6, D-17487 Greifswald, Germany
http://www1.physik.uni-greifswald.de

Emission at 844 nm – time averaged

Plasma induced emission of the discharge

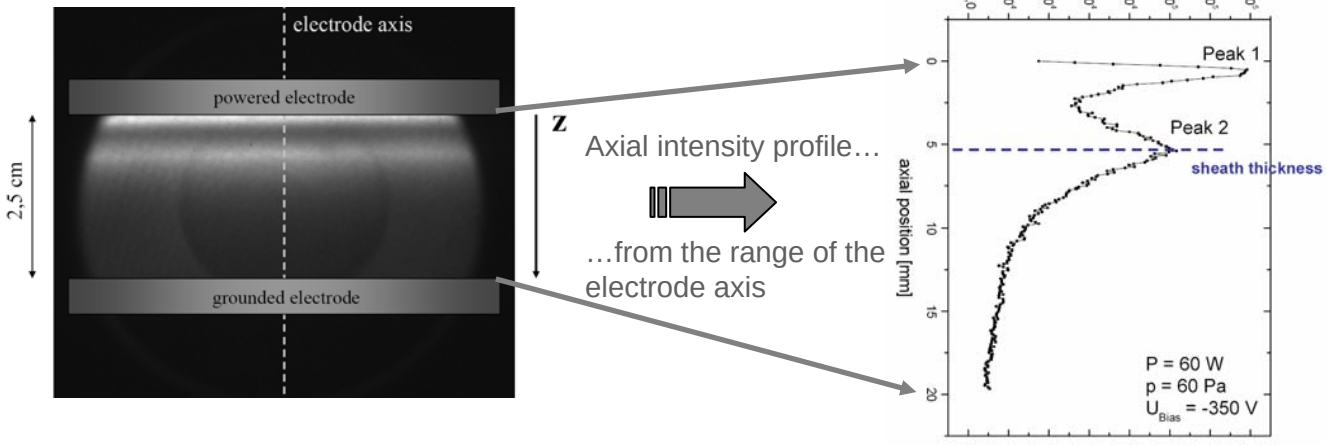

- Emission of atomic oxygen in two regions, mainly

  in front of the powered electrode (peak 1), and
  in the transition region rf sheath – bulk plasma (peak 2).

- Intensity maximum at 5 mm (peak 2) corresponds to the averaged sheath thickness

U_{Bias} - dependence

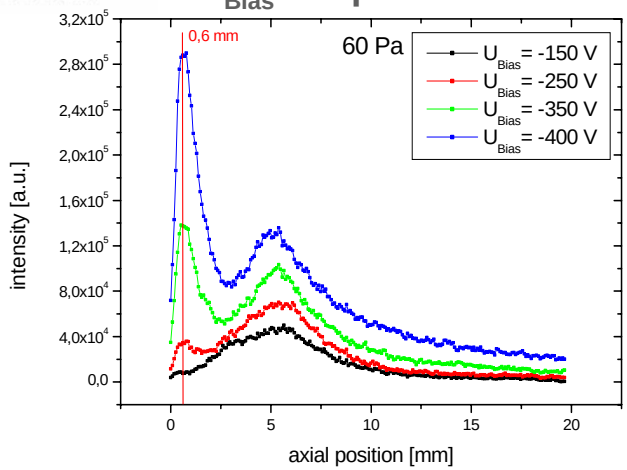

University of Greifswald, Institute of Physics
Low-temperature Plasma Physics, Prof. Dr. J. Meichsner
Felix-Hausdorff-Str. 6, D-17487 Greifswald, Germany
http://www1.physik.uni-greifswald.de

Axial intensity profiles (844 nm) – rf-phase resolved (T_{rf} ~ 74 ns)

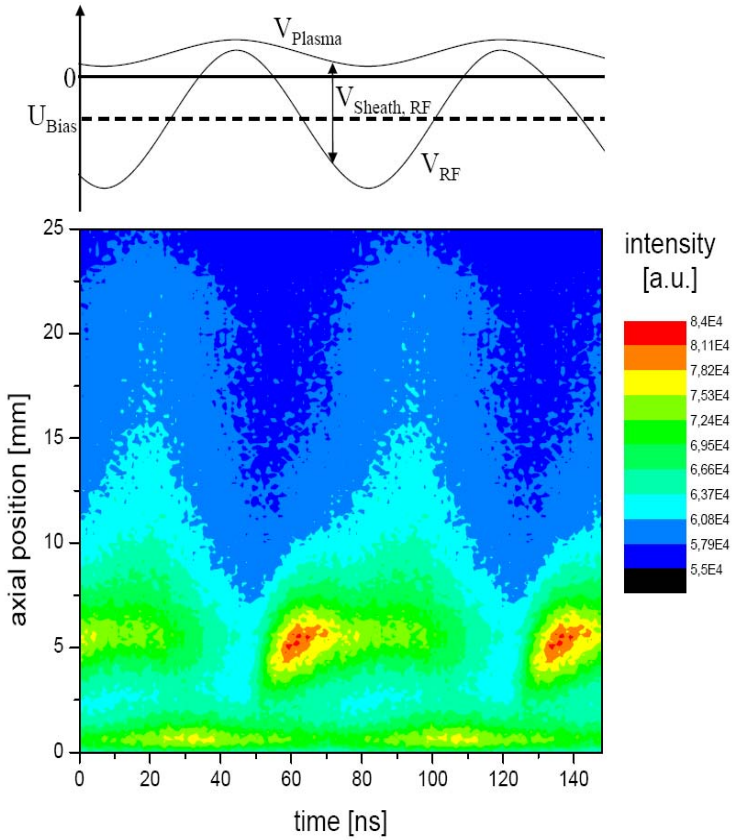

- Saw tooth-like modulation of emission intensity around 5 mm during rf-sheath expansion phase.

→ Excitation by electrons due to electron heating in the rf sheath.

- Reduced, phase shifted, and rather harmonic modulation in front of the rf electrode.

Assumption:

→ Excitation due to heavy particle collisions.

Lab3: Tunable diode laser absorption spectroscopy

Hoang Tung Do

Tunable diode laser with external cavity: Tunable diode laser absorption spectroscopy (TDLAS) can revolutionize many industrial processes by allowing highly specific, accurate, and non-intrusive real-time monitoring of species densities. TDLAS offers significant advantages over conventional spectroscopy. The spectral width of the laser radiation is much smaller than the width of the Doppler-broadened absorption profile. Sensitivity and signal to noise ratio are also increased in a TDLAS system because of a high-power coherent source. This improvement in sensitivity provides TDLAS the ability to detect and measure atom temperature and low concentrations using the Littrow configuration**.**

To obtain a spectally narrow single mode, we use an external cavity with optical feedback from a diffraction gratting. If the incident angle is such that the first order counterpropagates the laser output, the diffration from the gratting can be described by the equation:

$$2d\sin\theta = m\lambda$$

where θ is the so called Littrow-angle for a given wavelength λ, d is the line spacing of the grating and m is the order of diffraction. The wavelength of the external feedback has the lowest overall loss and succeeds in the resulting mode competition. The gratting therefore essentially filters the gain curve of the free-running (without gratting) diode laser.

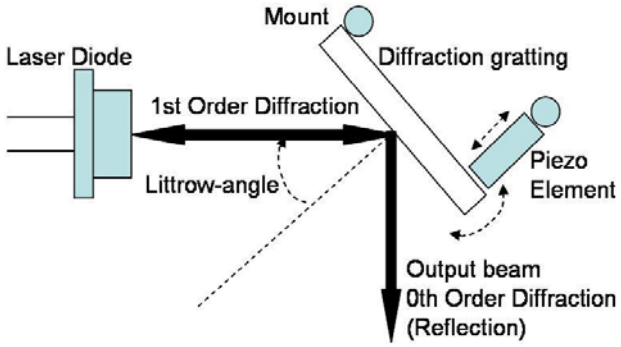

The diffraction gratting is attached to a mirror mount and the horrrontal tilt angle is controled by a piezo disk positioned in the mirror mount. Changing the applied voltage of the piezo element consequently change the angle of the gratting thus the output wavelength. The frequency can be swept over a wide range of up to 10GHz, which is more than adequate for many atomic physics applications.

TDLAS setup: The laser system consists of tunable single-mode diode laser and a control unit for diode temperature and diode current (Toptica DL 100). The laser light transverses a polarization filter and is directed onto a beam splitter. The transmitted light is registered by a photo diode behind a Fabry–Perot etalon to monitor the light frequency. The second light beam traverses the plasma chamber and is detected by a second photodiode.

From the absorption signal atom density and temperature can be calculated using the following equations:

$$n_a = \frac{4\pi\varepsilon_0 m_e c}{e_0^2 f\lambda_0}\sqrt{\frac{2kT}{\pi m_a}}\kappa_0 \text{ and}$$

$$T = \frac{\lambda_0^2 m_a}{8k\ln 2}\Delta\nu^2$$

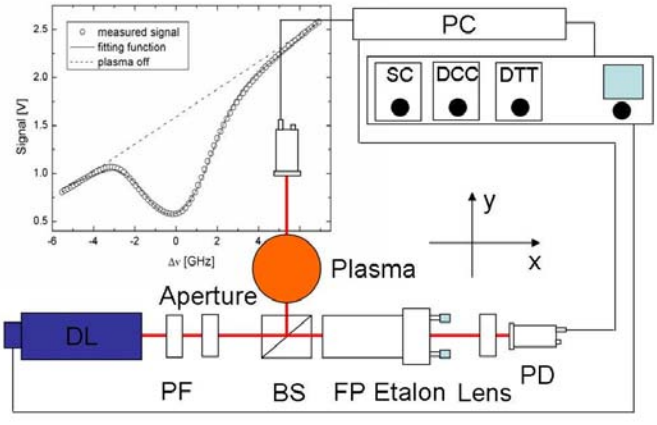

where κ_0 is the absorption coefficient in the centre of the profile, ε_0 is the dielectric constant, c the speed of light, m_e and e_0 are electron mass and charge, respectively, m_a is the neon atomic mass, k is the Boltzmann constant, λ_0 is the central wavelength of the investigated transition with the optical oscillator strength f and $\Delta\nu$ is the effective full-width at half maximum of the measured absorption profile.

Lab4: Fourier Transform Infrared Spectrometer

and

Infrared Spectroscopy using Quantum Cascade Lasers

Marko Hübner, INP

(a) Fourier Transform Infrared Spectrometer

A Fourier Transform Infrared Spectrometer (FTIR) is a Michelson interferometer with a movable mirror. By scanning the movable mirror over some distance, an interference pattern is produced that encodes the spectrum of the source (in fact, it turns out to be its Fourier transform).

In its simplest form, a Fourier transform spectrometer consists of two mirrors located at a right angle to each other and oriented perpendicularly, with a beamsplitter placed at the vertex of the right angle and oriented at a 45° angle relative to the two mirrors. Radiation incident on the beamsplitter from one of the two "ports" is then divided into two parts, each of which propagates down one of the two arms and is reflected off one of the mirrors. The two beams are then recombined and transmitted out the other port. When the position of one mirror is continuously varied along the axis of the corresponding arm, an interference pattern is swept out as the two phase-shifted beams interfere with each other.

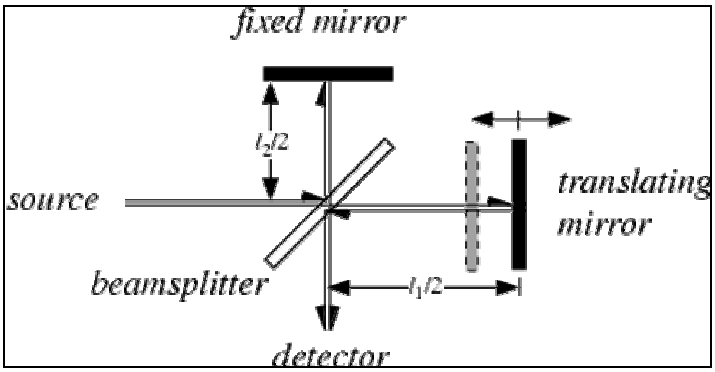

Fig 1 Participle sketch of a FTIR.

The interference pattern measured by the detector is shown in Fig 2. This signal is, in fact, the Fourier transform of the wanted spectrum.

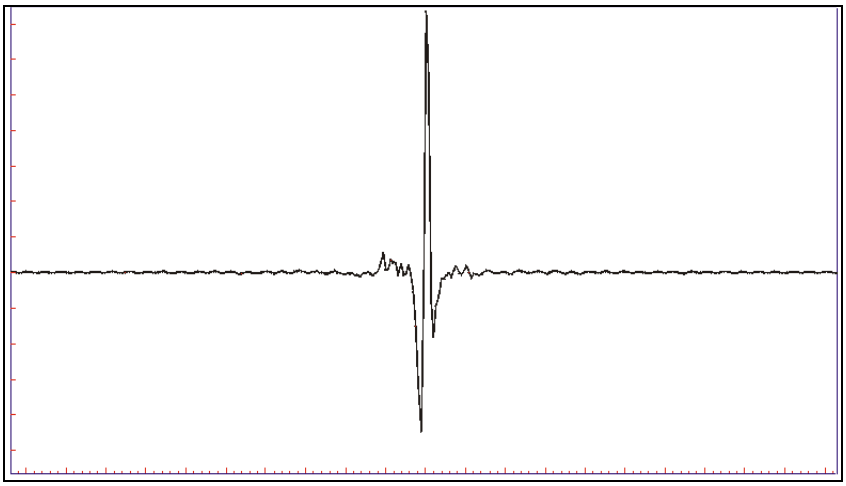

Fig 2 Typical shape of a recorded interferogram of the wanted spectrum.

The Fourier Transform of the interferogram leads to the spectrum of the measured gas, Fig 3.

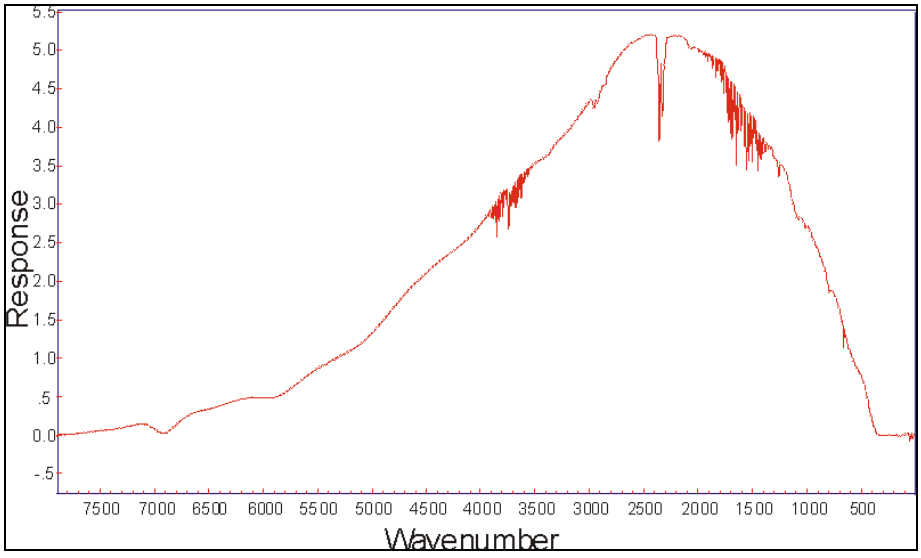

Fig 3 Example of a recorded spectrum.

Reference / Additional Information

http://en.wikipedia.org/wiki/Fourier_transform_spectroscopy
http://scienceworld.wolfram.com/physics/FourierTransformSpectrometer.html
http://www.ir-spektroskopie.de/spec/ftir-prinzip/index.html

(b) Infrared Spectroscopy using Quantum Cascade Lasers

A Quantum Cascade Laser (QCL) is a semiconductor based laser using quantum effects in stacks of thin layers. Such a QCL consists of about 20 laser periods. Each period is a pack of semiconductor layers, where each layer is a semiconductor alloy. If a voltage is applied, the conduction band diagram acquires a staircase like shape. A typical "Energy versus Distance" diagram of such an arrangement is shown in Fig. 1.

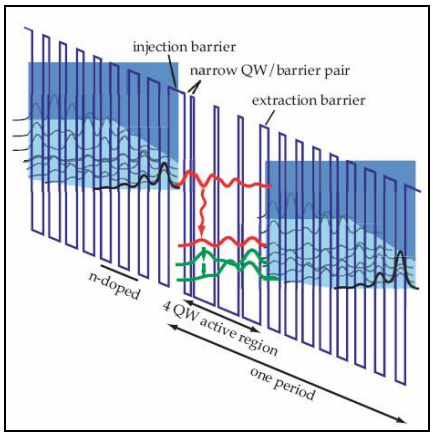

Fig. 1 Schematic quantum well (QW) structure of a QCL.

QCL work parameters: operated at near room temperature
output power > 1 mW
linewidth ≤ 0.01 cm^{-1}

There are several methods to drive a QCL. One is called: **Inter Pulse Mode**.
It works as follows:
A pulsed driving voltage is applied with a frequency f_{QCL} between 10 to 100 kHz and a pulse width of 10 to 50 ns. Additionally, a ramp shaped voltage is fed to the QCL with a period of ms. Hence, the laser changes its temperature and therefore the emitted laser frequency is tuned slightly, Fig. 2.

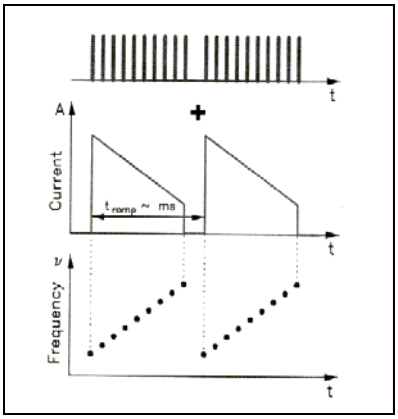

Fig. 2 Pulsed voltage (top), ramp shaped voltage (middle), tuned laser frequency (bottom) of a QCL.

As a result the following absorption spectrum can be measured.

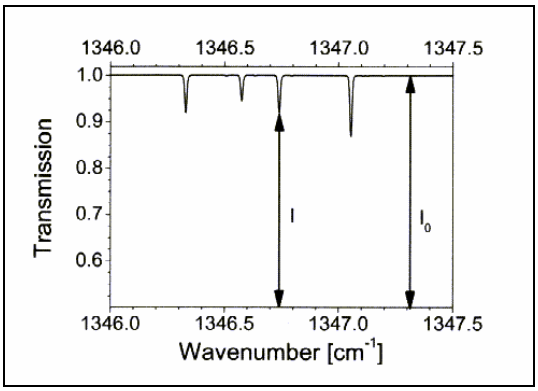

Fig. 3 Example of a room temperature spectrum of 100 ppm CH_4 at 5 mbar and 24 m absorptions length.

If the pressure p and the temperature T of the gas under investigation are known the number density n of the species can be determined by integration over the absorption line using Lambert Beer's law

$$\int_{line} \ln\left(\frac{I_0(\nu)}{I(\nu)}\right) d\nu = nSL$$

where I_0 and I are intensities (Fig. 3), L is the absorption length and ν is the frequency. The line strength S is tabulated in the HITRAN [4] database. The relative concentration or mixing ratio x of the gas can then be calculated by

$$x = \frac{n}{n_{tot}} = \frac{n}{p} k_B T$$

where n_{tot} is the total number density given by the ideal gas law, i.e. given by the pressure p, the temperature T and Boltzmann's constant k_B.

References:

[1] S. Welzel; INP 2007
[2] S. Blaser; www.alpeslasers.ch
[3] J. Faist et al.; SCIENCE, Vol. **264**, 1994
[4] http://cfa-www.harvard.edu/HITRAN

Lab5: Dielectric barrier discharge

Abhijit Majumdar

A dielectric-barrier discharge (DBD) represents a self-sustained non-equilibrium electrical gas discharge that can be operated at pressures of the order of 1 bar. Dielectric-barrier discharges are characterised by insulating layers on one or both electrodes or on dielectric structures inside the discharge gap. At atmospheric pressure the physical processes resemble those in transient high-pressure glow discharges. The discharge can be reliably operated up to high power levels in the megawatt range, a property which is of importance for industrial applications.

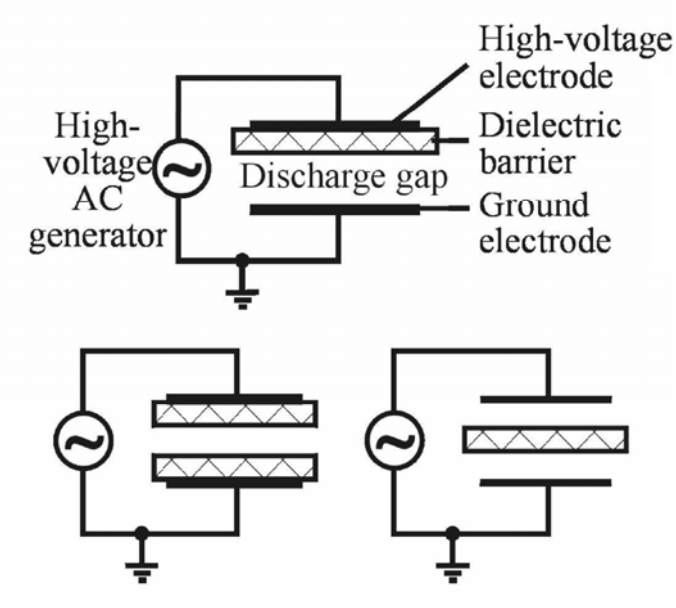

If an ac voltage is applied to one of the electrode with both covered by a dielectric layer, a discharge will appear in the gas gap which is so called dielectric barrier discharge (DBD) or barrier discharge. The interesting features of our apparatus are the construction of the dielectric electrodes made of Alumium oxide or Alumina (Al_2O_3) and glass; and the generation of high ignition voltage from the spark plug transformer taken from car. The DBD set up is the assembly of several components which are following:

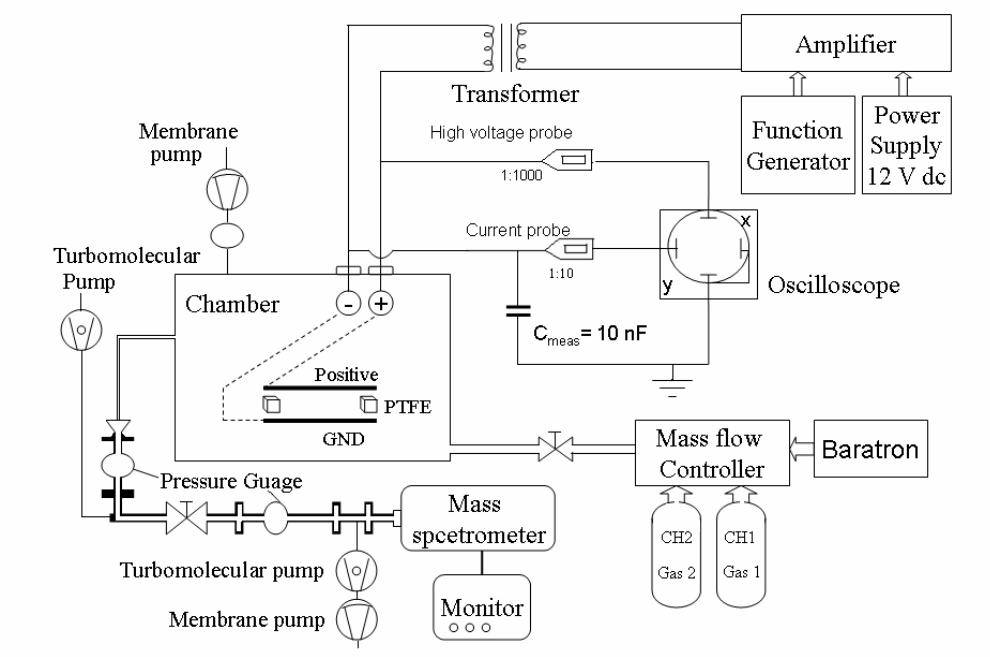

1. Reaction chamber and electrodes configuration, 2. Electrical inputs, 3. Gas flow System, 4. Pumping system, 5. Probe measurement, 6. Spectrograph.

The reaction chamber is made of stainless steel with volume of 3.32 dm^3. The two electrodes are made from Ag plates with a length of 8.3 cm, width 3.3 cm, and thickness 0.15 cm. The Ag plate is placed in a rectangular shape Plesi-glass holder or container and both the Ag electrodes are covered by dielectrics: the upper (powered) electrode is covered with aluminium oxide ($\varepsilon \sim 10$); the lower (grounded) electrode with a glass plate ($\varepsilon \sim 3.8$). The air gap between two electrodes is variable, depending on the experimental condition and it is insulated by Teflon (PTFE, polytetra fluoreoethylene) insulation. The chamber is pumped by a membrane pump down to a base pressure of about 10 mbar. The experiments were performed at a pressure of 250--400 mbar and with varying different gas ratios. Membrane Vacuum pump (Pfeiffer, GmbH, Germany) is used to evacuate the reaction chamber up to 1 mbar. Turbo molecular pump (Pfeiffer, TCP 121) is introduced at the end of the capillary tube to create the pressure gradient in between chamber and mass spectrometer end. Gas composition of stable reaction products only was detected by a mass spectrometer (Balzers QMS 200) pumped by a turbo molecular pump (Pfeiffer TSU 062H) to a base pressure of about 1×10^{-8} mbar. Gas flow system consists of, (i) Baratron (MKS Instrumets, USA) (ii) Multiple Mass flow controller (MKS Instruments, USA) and (iii) Gas cylinder (CH_4, Ar, N_2, H_2, He etc). Out of four channels of Mass flow controller, only two channels are used in the prospective experiments. The electrical system accompanied by, (i) Power supply, (ii) Function generator, (iii) Amplifier (HURRICANE, GmbH, Germany) and (iv) Spark plug transformer. The power supply is 12 V dc, is used to bias the audio amplifier for the threshold potential. Function generator or frequency generator delivering a sinusoidal output that is fed into an audio amplifier. The amplifier can be operated at up to 500 W. Mass spectrometer (Balzers QMS 200) is connected with the reaction (plasma) chamber through a capillary tube of length 103 cm and inner diameter 0.01 cm. A pressure of 10^{-2} mbar at the entrance to the mass

spectrometer is maintained during the experiments with the help of a second turbomolecular pump (Balzers 071P). Gas composition of stable reaction products only was detected by a mass spectrometer (Balzers QMS 200) pumped by a turbomolecular pump (Pfeiffer TSU 062H) to a base pressure of about 1×10^{-8} mbar.

Lab6: Magnetron plasma source

V. Stranak

Devices called magnetrons are primarily used for physical vapour deposition (PVD) processes. Magnetron principles are known for a long time since 1978 from works by [1,2] in planar or cylindrical configuration, respectively. Magnetron sputtering deposition sources are now widely used in industry because of their simple technology, economic acceptability and easy alterable physical conditions. Magnetron technology as well as magnetron plasma diagnostic is, however, continuously developing because new advanced films with prescribed physical and functional properties are needed.

A typical planar magnetron sputtering system consists of a planar cathode (sputtering source or target) parallel to an anode surface (usually grounded), which serves as a substrate holder. The cathode assembly consists of the source material, dependent on the deposited layer, directly connected with the backing power electrode. Magnets are placed below backing electrode. The structure of the magnetron is shown in Fig.1.

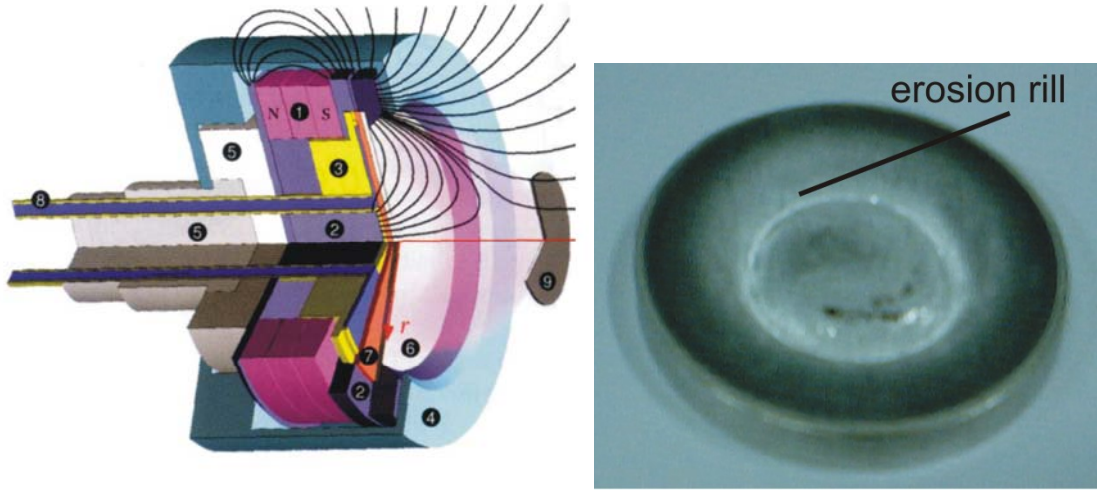

Fig.1. The cross-section of the magnetron (1 magnets, 2 magnetic circuit and target clamp, 3 coolant chamber, 4 shielding, 5 insulator, 6 target, 7 cooper meant, 8 water tube cooling, 9 substrate) and photo of real used Ti target with visible erosion rill.

If the negative voltage is applied on the cathode and the pressure is low enough, a glow discharge is formed. Negative particles (mainly electrons) of a dc glow discharge are trapped by external magnetic field, which in a certain region above the cathode runs parallel to the cathode surface. Such configuration increases electron density in a localized zone. The increased electron concentration leads to higher ion production through ionisation collisions. Radial current distribution is peaked at the radius at which the magnetic field is tangent to the cathode plate [3]. Relatively strong electric field between the positive glow plasma and the cathode accelerates ions towards the cathode, where they sputter the cathode material. The most intensive sputtering of the target is visible as an erosion rill called race-track; see Fig.1.

The external magnetic field is essential feature of magnetrons. Planar magnetrons can be operated with two types of magnetic fields corresponding to balanced (BLM) [3] and unbalanced (UNB) mode [4], see Fig.2. Generally, it is difficult to precisely distinguish between modes. The characteristic feature of balanced mode is magnetic field lines well confined around the cathode. The electron loss is reduced to minimum. The basic principle of the unbalanced magnetron is to allow release of electrons from the magnetic trap in order to create ionization away from the magnetron cathode near by substrate. Sheridan et al. showed that electrons escape from plasma up the "chimney" along the axis of cathode in UNB magnetron [5]. On the contrary, their earlier simulations [6] show that electrons in BLM magnetrons escape radially outward.

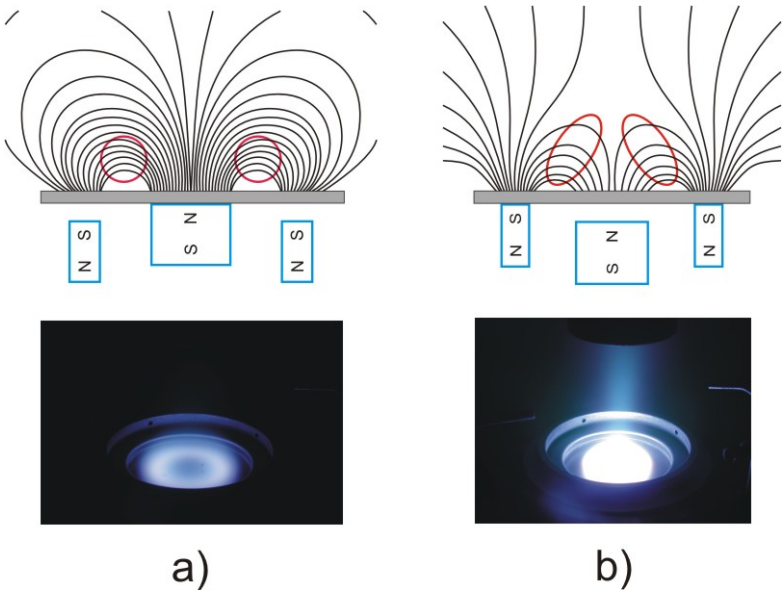

Fig.2. The magnetic field lines and photos of magnetron discharge operated in a) balanced, b) unbalanced mode.

Generally it is difficult to characterize physical and technical parameters of magnetrons because of wide range of their experimental modifications. However, typical overall parameters of dc planar magnetrons are specified below. Negative voltage bias in order of several hundreds volts (usually up to -1.000 V) is applied on the cathode - the target. The diameter of the circularly shaped target is usually from 60 up to 200 mm with the thickness about 7-10 mm. Target is made of material to be deposited - mainly Ti, In, Ta, Al, Cu, Zr and other species. As buffer gases are frequently used inert gases (e.g. Ar) with reactive component(s) (e.g. O_2, N_2,) for creation of -oxide or –nitride layers.

With the view to increase efficiency of technological depositions the conventional magnetrons are converted to pulsed systems. This means that the instant discharge current in the active pulse can be very high but the average discharge current is low and has similar magnitude as in the systems working in continuous mode. The next important reason of using pulse magnetrons is discharging of dielectric layer or clusters formed on the cathode target during reactive sputtering process of dielectric films. The modulation frequency is typically selected in a wide range from 100 Hz up to 350 kHz. Another way how to increase efficiency or quality of the deposited layers lie in using large, shape-complicated targets (e.g. rectangular), additional ionisation component (RF, MW), movement of substrate during deposition etc.

[1] R. K. Waits, J. Vac. Sci. Technol. **15(2)**, (1978), 179.
[2] J. A. Thornton, J. Vac. Sci. Technol. **15(2)**, (1978), 171.
[3] A. E. Wendt, M. A. Lieberman, H. Meuth, J. Vac. Sci. Technol. **A6 (3)**, (1988), 1827.
[4] B. Window, N. Savvides, J. Vac. Sci. Technol. **A4(3)**, (1986), 196.
[5] T. E. Sheridan, M. J. Goeckner, J. Goree, J. Vac. Sci. Technol. **A8(1)**, (1990), 30.
[6] J. E. Miranda, M. J. Goeckner, J. Goree, T. E. Sheridan, J. Vac. Sci. Technol. **A(8)**, (1990), 1627.

Lab7: X-ray Photoelectron Spectroscopy (XPS)

Stefan Wrehde

1. Basics

XPS (X-ray Photoelectron Spectroscopy), which is also known as ESCA (Electron Spectroscopy for Chemical Analysis), is a widely used technique for surface analyses. The advantage of XPS compared to other surface analysis techniques is that it provides information about the chemical composition of the surface as well as about chemical boundaries. The detection limit is roughly 1%.

The method is based on the emission of photoelectrons from the examined sample, which is exposed to x-ray radiation with the energy $h\nu$. Commonly used x-ray sources are Mg Kα (1253,6 eV) and Al Kα (1486,6 eV).

The kinetic energy E_k of the electrons is given by the difference between photon energy and binding energy at surface E_b :

$$E_k = h\nu - E_b . \qquad (1)$$

Since every element has a unique set of binding energies XPS can be used to identify elements in a surface and determine their concentration. Additionally very often the chemical boundaries can be detected.

The information depth of XPS measurements is limited by the mean free path length λ_e of the photoelectrons (few nm) and is independent of the significantly bigger incidence depth of the x-rays (1...10 μm). Only electrons leaving the surface without collisions carry the element's characteristic kinetic energy and contribute to a sharp peak in the spectrum. Otherwise they raise the level of the background at binding energies higher than the peak energy.

2. Data interpretation

An XPS-spectrum is showing the number of electrons versus binding energy at surface (or kinetic energy).

A typical XPS-spectrum of a Si-wafer (100) is shown in Fig. 1. In this overview spectrum one can see the peaks caused by the electrons of the O 1s-,O 2s-, C 1s-, Si 2s- and Si-2p-levels.

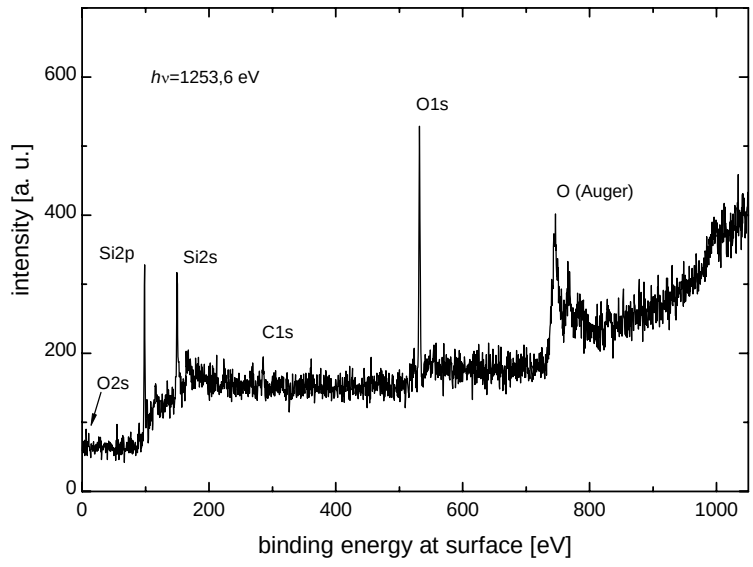

Fig. 1 Typical XPS-spectrum of a Si-wafer.

The interpretation of an XPS-spectrum starts with identifying the peaks of the elements C and O which can be found on almost any sample. After this the strongest lines and their auxiliary are identified. From their energetic positions it is possible to assign them to the elements in the layer surface by comparing the peak positions with reference measurements from literature. The assignment of a peak position to an element is not always definite. Under certain circumstances it is possible to assign more then one element to one single peak. To definitely identify an element it is necessary to detect all associated peaks.

In addition to element identification it is very often possible **to detect the chemical boundaries** if the participating elements have different electronegativities. In this case a chemical binding leads to a shift of the electronegativities resulting in a shift of the assigned XPS-peak, the so-called *chemical shift*. For example, the Si 2p Peak of a pure Si surface can be found at E_b = 99,15 eV. If the surface is oxidised, silicone appears as SiO_2 and the (or an additional) 2p peak is situated at $E_b \approx$ 103,4 eV (see Fig. 2).

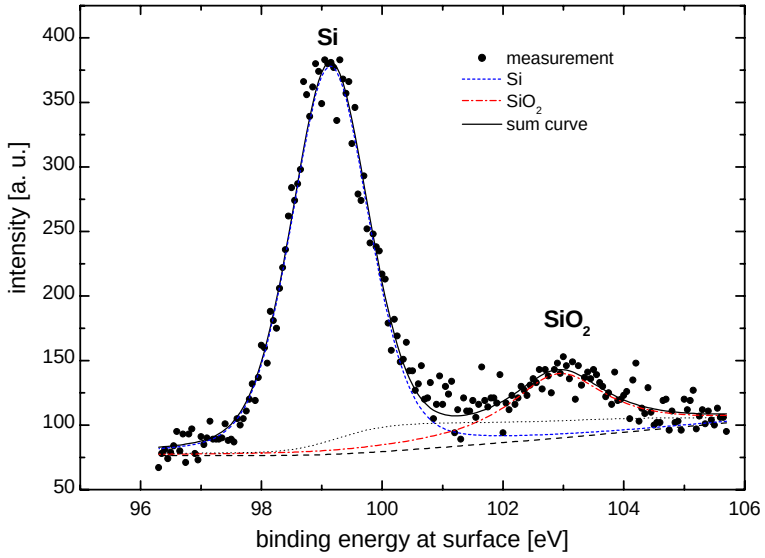

Fig. 2 *Detailed XPS-spectrum of the Si 2p Peaks of a Si-wafer*

A quantitative analysis of the layer composition is possible via the peak areas. Because of the element dependent emission probability of a secondary electron the peak areas have to be normalised using sensitivity factors (*ASF*). By means of the normalised peak areas the quantitative layer composition can be calculated by:

$$C_j = \frac{A_j / ASF_j}{\sum_i A_i / ASF_i} \qquad (2)$$

(C_j – concentration of element j, $A_{i,j}$ – peak area of element i or j, $ASF_{i,j}$ – sensitivity factor of element i or j)

To obtain a depth profile of the layer composition by means of XPS there are different options. Variation of the angle between sample normal and detector at constant λ_e leads to different information depths from the surface down to approximately 3 λ_e. Thus it is possible to obtain a depth profile of the layer composition without destruction of the sample (ARXPS). Furthermore detailed analyses of the background may allow conclusions on the layer composition profile close to the surface. To obtain depth profiles through the whole layer it is necessary to gradually remove the layer e.g. by means of sputtering. A major problem of this technique is the fact that the different elements may be sputtered with different yields (so-called selective sputtering) leading to a change of the original profile.

Lab8: Diagnostics of plasma deposited layers by x-ray diffractometry

Marion Quaas

Introduction

Grazing incidence X-ray diffractometry

The most frequently used and the most important problem in thin film analysis is to prove the existence of a desired phase after film deposition or to find out which phase or phases were formed.
X-ray diffractometry has been established as a well-suited tool for investigations of physical, chemical and crystallographic properties. The x-ray methods are non-destructive techniques, therefore a sample can be reused, and can be measured with other techniques, such as XPS, AFM or FTIR.
As a result, x-ray techniques are applied by researchers in a wide range if disciplines.
The observation of X-ray diffraction from very thin films is often hampered by weak diffraction intensities due to smallness of the diffraction volume. Thin polycrystalline films can be studied with advantage in the highly asymmetric Bragg case. In this technique the diffraction volume can be increased by decreasing the angle of incidence.
In grazing incidence X-ray diffractometry (GIXD) the substrate reflections are suppressed and the film intensities increase. The reflection positions are equal in the Bragg-Brentano geometry (BB) and in the asymmetric Bragg case (GIXD).

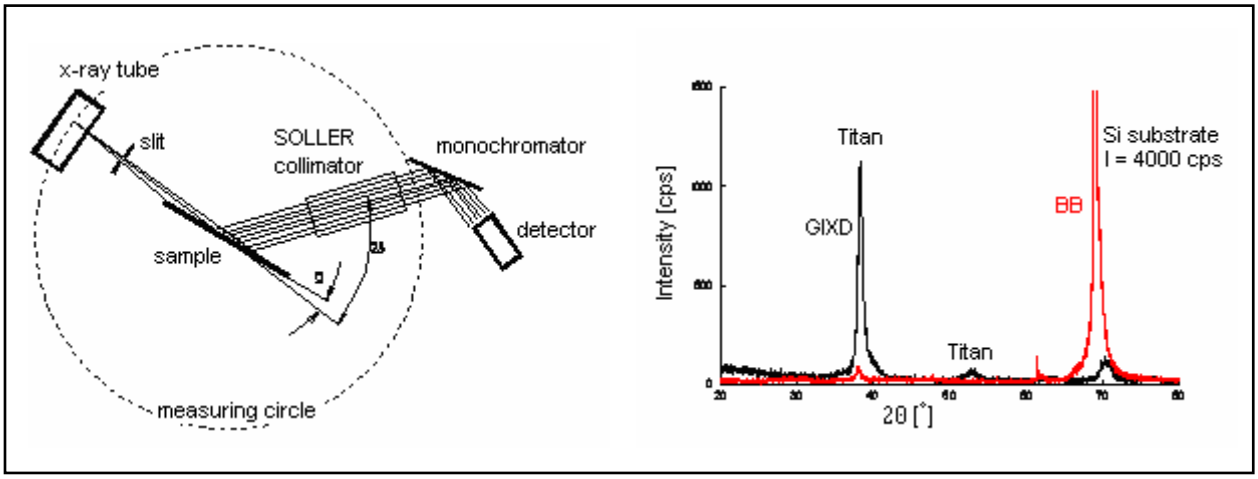

Figure 1 Schematic illustration of grazing incidence x-ray diffractometry (asymmetric Bragg case) and comparison of measurements of a thin Ti film on Si substrate in GIXD (black) and BB (red) geometry

Phase identification

X-ray patterns are compared directly with the PDF pattern (Powder diffraction file, ICDD). This database contains about 300.000 entries. The program *Pcpdfwin* supports search/match routines, determined by knowledge of what is expected or by other search criteria. Simple searches can be made on chemical formula, chemical name using the alphabetical index. For samples with no chemical information available the Hanawalt search schemes must be used.

Exercise

Take up the diffraction pattern of a plasma deposited thin film!
Identify the compounds present in the film!